

Chapter 2

Nature of the Electronic Charge Carriers Involved in Triboluminescence

Friedemann T. Freund

2.1 Introduction

Luminescence describes the emission of light from matter, mostly solids, that is not generated by heat. Different actions can cause luminescence. Triboluminescence, for instance, is caused by mechanical action. Some major questions arise: How does mechanical action produce luminescence and why can it be observed in some materials but not in others?

When solids are subjected to compressive or tensile forces, they deform. At first, within the elastic range, deformation is proportional to the applied force. At higher stresses deformation becomes non-linear. Eventually the solids will fracture creating new surfaces.

Microscopically, fracturing means that interatomic bonds are broken as a fracture propagates through the solid medium creating two opposite surfaces, which begin to separate. Because of the stochastic nature of any fracture event these fracture surfaces will contain atoms/ions with dangling bonds and will carry patches of charges of opposite signs. As the surfaces separate, electric (E) fields develop, which can be high to very high. These E fields momentarily accelerate electrons and ions emitted from the fracture surfaces. The E fields are particularly high at the tip of propagating cracks—high enough to accelerate electrons and ions over short distances to such high energies that they impact-ionize gas neutrals, creating additional electrons and ions, and causing avalanche electric discharges. Such discharges produce bursts of light with spectra extending through the visible (VIS) into the ultraviolet (UV) and even into the X-ray region [1]. The high-energy portion of this light will surely interact with the bulk of the solid and initiate secondary reactions.

F.T. Freund (✉)

GeoCosmo Science Center – NASA Ames Research Park, Bldg 19,
Suite 1070-I, Moffett Field 94035, CA, USA
e-mail: friedemann.t.freund@nasa.gov

Interesting from the viewpoint of triboluminescence are cases when the emitted light is colored and does not only come from the narrow gap between the fracture surfaces or from the fracture surfaces themselves, but from the inside of the bulk. Often triboluminescence is produced by relatively gentle mechanical actions such as rubbing or tumbling. Though rubbing or tumbling may cause spallation and microfractures on very small scales, they are a far cry from the highly energetic processes that take place during macroscopic fracture. If there is persistent light emission coming from within the bulk during rubbing or tumbling, we have to consider mechanisms, by which relatively large bunches of energy are created with very small input of mechanical energy, flowing from the surface or near-surface region, where the mechanical action had taken place, into the underlying bulk.

This chapter deals primarily with oxide materials. It reports on a specific type of point defects in oxide materials that has been consistently overlooked by the scientific community: peroxy defects, where oxygen changes its valence from 2— to 1—. Peroxy defects occur in many oxides and in silicates. They occur in rocks. It will be argued here that peroxy defects and the highly mobile positive hole charge carriers, which they engender, play a major role in energy transfer processes that allow triboluminescence to occur at sites, which are some distance away from the sites of the mechanical action. At the end of this chapter the insight gained from studying peroxy defects and positive holes in oxide materials will be extended to non-oxide materials.

2.2 Peroxy—The Stealth Defects

2.2.1 *Band Structure and Electronic Charge Carriers*

Any form of luminescence requires the formation of excited states, commonly electronically excited states, and their de-excitation via radiative transitions. If the light emission falls into the visible (VIS) range, their photon energies range from 1.65 eV in the red (750 nm) to 3.1 eV in the violet (400 nm). Since kT , the mean thermal energy¹ at 300 K, is only 25 meV, the energy emitted over this spectral region is 25–65 times the amount of energy available through kT . Two questions thus arise: (1) where does the energy come from that can lead to the emission of photons in the VIS region and (2) how does this energy travel through the solid medium from the site of mechanical action to the site of photon emission.

To start it may be good to look at some fundamental issues regarding electronic charge carriers in solids. Figure 2.1a and b sketches the valence and conduction bands for semiconductors and insulators, respectively. The difference between the two classes of materials lies in the width of the bandgap E_g . In a semiconductor E_g is sufficiently narrow for some electrons from the fully occupied valence band to be

¹ With k being the Boltzmann constant and T the absolute temperature.

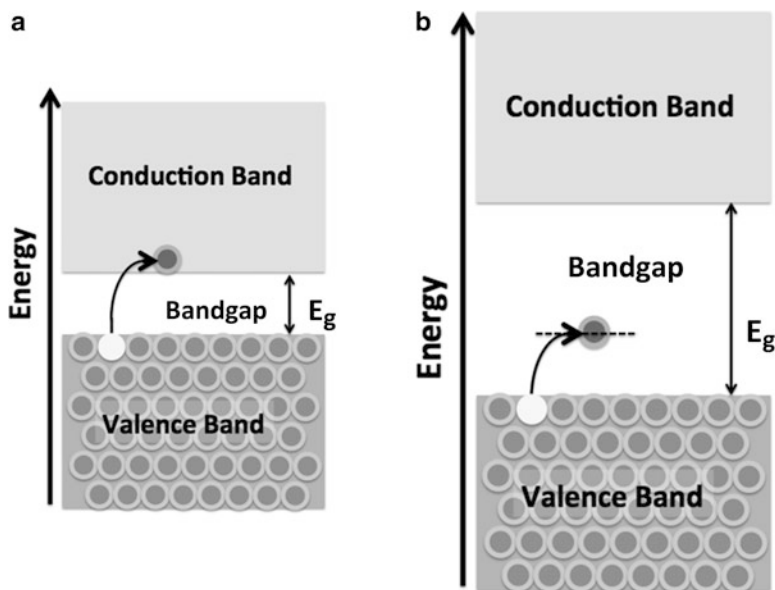


Fig. 2.1 (a, b) Schematic representation of the band structure of (a) a semiconductor and (b) an insulator, both with fully occupied valence bands. E_g is the width of the band gap. The arrows indicate that electrons can be thermally activated (by kT) into the conduction band or into impurity levels in the band gap, respectively. Figure b indicates that, when E_g is much wider than the thermal energy kT as is the case in insulators, electrons cannot be thermally activated to the conduction band. However, if impurities create energy levels in the band gap that can act as acceptors, electrons from the valence band can be promoted to these impurity levels. Unless their density is so high that their wave functions partly overlap, electrons on those impurity levels will be localized and do not contribute to the electrical conductivity

thermally promoted into the conduction band due to the thermal energy kT , where k is the Boltzmann constant and T the absolute temperature. The promotion of an electron into the conduction band leaves a defect electron in the valence band, also known as a hole [2]. In the intrinsic case the ratio of the number of electrons in the conduction band n' and the number of holes in the valence band n^* is 1. Electrons and holes are both mobile, albeit with different mobilities, μ' and μ^* , respectively, with electrons being typically more mobile than holes.

2.2.2 Peroxy Defects in Oxide Materials, Minerals, and Rocks

The O^{2-} anions in oxide materials are commonly assumed to be in the 2- valence state and in the 2- valence state only. However, oxygen can exist in two valence states, 1- and 2-. A peroxy defect consists of two oxygen anions oxidized from

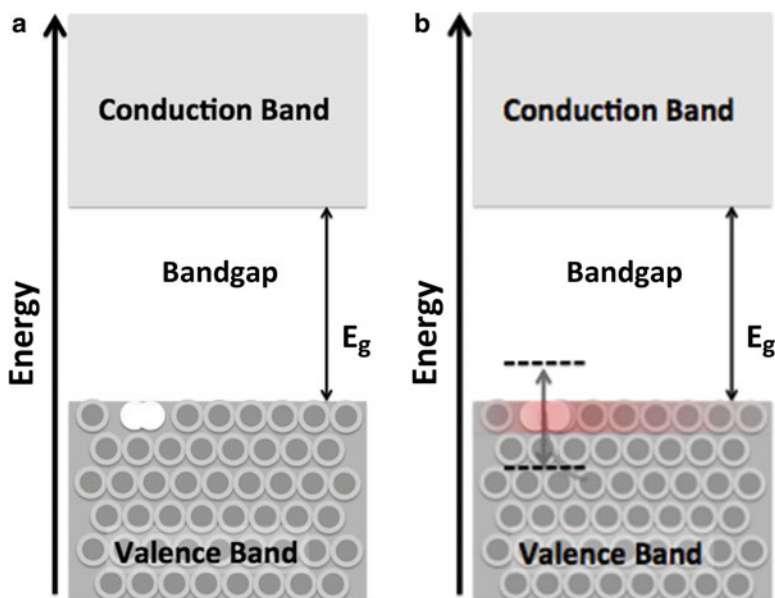


Fig. 2.2 (a) Schematic representation of the effect of a peroxy defect on the energy surface of the valence band of an oxide insulator. The majority $2-$ oxygen anions are shown in *dark gray*. The white dumbbell represents a dip in the energy surface of the valence band due to the presence of a peroxy defect. (b) When a peroxy defect becomes activated, it generates two states: an electron that remains trapped in the broken peroxy bond and a hole that delocalizes over many neighboring O^{2-} and becomes as mobile charge carrier

$2-$ to $1-$. Figure 2.2a and b sketches a situation, where a peroxy defect is introduced into an oxide material. It is equivalent to two holes trapped on two adjacent O^{2-} sites. Since the -1 valence state primarily affects energy levels of O $2sp$ symmetry at the upper edge of the valence band, peroxy defects manifest themselves by a local dip in the energy surface of the valence band as indicated in Fig. 2.2a.

When the $O^- - O^-$ bond breaks, an electron can be transferred into the broken peroxy bond from an outside O^{2-} . This electron gets trapped in the broken peroxy bond, occupying an energy level slightly below the edge of the valence band as indicated by lower dashed line in Fig. 2.2b. By symmetry an empty energy level is created slightly above the edge of the valence band, as indicated by the upper dashed line in Fig. 2.2b. The donor O^{2-} turns into an O^- , i.e., into a defect electron in the O^{2-} sublattice, e.g., a hole. As will be argued further below this hole state tends to delocalize over many O^{2-} neighbors as indicated by the reddish hue in Fig. 2.2b. Because of this and of other rather remarkable properties associated with this hole state in the oxygen anion sublattice, it has been given the name “positive hole” [3].

Much of what follows from here onward derives from the noteworthy properties of positive holes, which the peroxy defects release when they break up. A major point will be to examine how peroxy defects and positive holes contribute to luminescence phenomena and specifically to triboluminescence.

2.2.3 *Nature of Electronic Charge Carriers, Electrons, and Holes, in Insulating Oxide Materials*

Peroxy defects are a family of point defects in oxide materials that have not received the attention they probably deserve. Though they seem to be ubiquitous across a wide range of oxide materials and rock-forming minerals, their presence has been largely overlooked.

Peroxy defects consist of pairs of oxygen anions, which have changed their valence from the usual $2-$ state to $1-$, where O^- is more oxidized than O^{2-} . The two O^- are covalently bonded, forming a very short O^-O^- bond, only ~ 1.5 Å as compared to the usual 2.8 – 3.0 Å distances between adjacent O^{2-} . Though the activation energy to dissociate peroxy bonds is relatively high, on the order of 2.4 eV in MgO [4] and probably similar in other oxide matrices, they are also quite labile. They break up, when an electron is transferred from some nearby O^{2-} into the peroxy bond and becomes trapped, leaving one O^- with the broken peroxy bond. This O^- is stationary, while the donor O^{2-} turns into O^- and becomes a mobile positive hole charge carrier, which can move away from its point of origin. There is strong evidence that the wave function associated with this mobile O^- state, e.g. with the positive hole, is highly delocalized over the O 2sp-type energy levels that form the upper edge of the valence band [5, 6]. The peroxy dissociation can of course reverse by the mobile hole recombining with another mobile hole or with a defect-bound O^- .

O^- have a strong propensity to take over an electron to return to the O^{2-} state. Thus they act as oxidizing agents. When positive holes roam through the bulk, they can interact with transition metal cations and participate in charge transfer processes. This is the reason why positive holes are interesting actors in the context of luminescence, including triboluminescence.

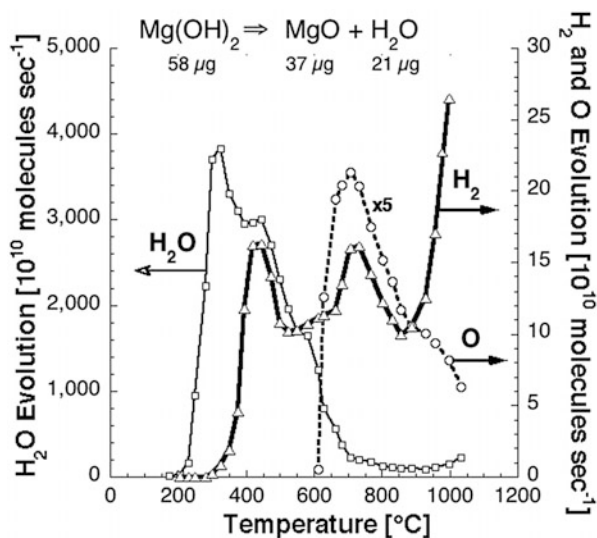
Since peroxy defects and positive holes have not been widely discussed in the literature yet—except in papers by the present author—the work presented here and the references quoted will primarily tap this source of information. Magnesium oxide, MgO, played a major role in the discovery of peroxy defects and positive holes. Subsequently peroxy defects and positive hole-type charge carriers have been shown to also exist in other oxide materials, including silicates. There is evidence that similar defects also exist in non-oxide materials.

2.3 Discovery and Validation of Peroxy Defects

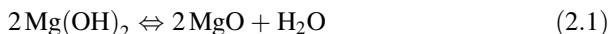
2.3.1 *Formation of Oxygen Anions in the 1– Valence State*

Peroxy defects were first observed in MgO, the structurally simplest oxide, face-centered cubic. As a main group element Mg has only one chemically stable

Fig. 2.3 During thermal decomposition of $\text{Mg}(\text{OH})_2$, made from ultrahigh-purity MgO , H_2O is not the only gas that evolves but also H_2 and atomic O [7]

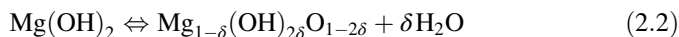


oxidation state, 2+. The thermal decomposition of $\text{Mg}(\text{OH})_2$ should produce MgO plus H_2O as the only gaseous product:



However, during the thermal decomposition of ultrahigh purity $\text{Mg}(\text{OH})_2$ substantial amounts of H_2 were observed [7]. Figure 2.3 shows that the reaction started with H_2O evolving first, around 200 °C. After the decomposing $\text{Mg}(\text{OH})_2$ had begun to recrystallize to nano-sized MgO [8], H_2 began to evolve around 300 °C with maxima around 450 °C and 750 °C, the latter accompanied by the evolution of atomic O starting at 600 °C. Note: The H_2 recorded above 900 °C does not come from the MgO sample but from the walls of the fused silica tube in which the decomposition reaction was conducted.

Here are more details. The dehydroxylation of the $\text{Mg}(\text{OH})_2$ begins with the loss of H_2O :



During this initial step the hexagonal structure of $\text{Mg}(\text{OH})_2$ is preserved, while H_2O molecules are removed from between the layers, probably up to 90 % of the total OH^- [9]. The resulting highly defective, hexagonal structure then becomes unstable and collapses to form nanosized cubic MgO , still retaining a high concentration of residual OH^- [10]. As Fig. 2.3 shows the H_2 evolution begins after the cubic MgO nanocrystal had started to form [9].

The face-centered cubic MgO structure offers only a few sites for OH^- to be incorporated as depicted on the left of Fig. 2.4 [11]. There are three types of “impurity” OH^- :

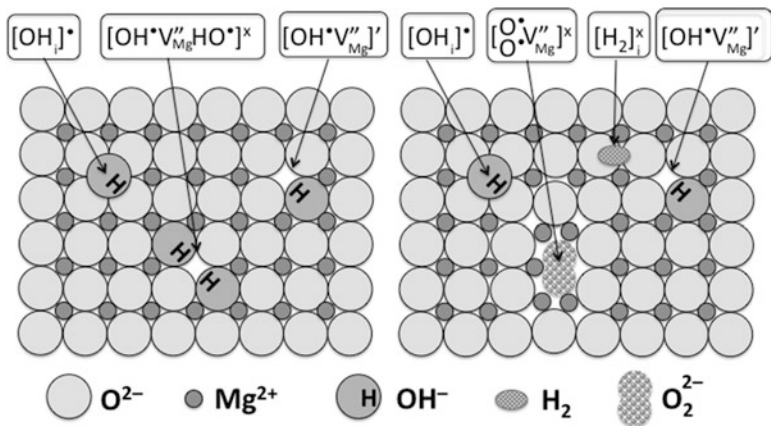
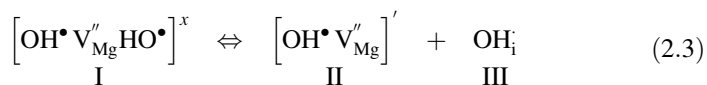


Fig. 2.4 Projection of the different crystallographically allowed “impurity” OH^- onto the (110) plane of MgO . *Left*: before redox conversion of OH^- pairs. *Right*: After redox conversion of OH^- pairs and formation of a peroxy anion and molecular H_2 . *Top row*: Kröger-Vinck point defect designation for the different defects formed

- I. OH^- pairs adjacent to Mg^{2+} vacancy sites (expected to be most abundant).
- II. Single OH^- at Mg^{2+} vacancy sites (expected to be less abundant).
- III. OH^- with the O–H vector pointing into an interstitial site (also less abundant).

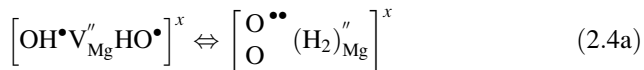
To describe these impurity OH^- we use the Kröger-Vinck point defect nomenclature [12],² where OH^- pairs at Mg^{2+} vacancy sites (I) are written as $[\text{OH}^\bullet \text{V}_{\text{Mg}}'' \text{HO}^\bullet]^\times$, with two hydroxyl H^+ at O^{2-} sites compensating for the 2– charge associated with the Mg^{2+} vacancy. This charge-compensated OH^- pair defect (I) should be most abundant. It can dissociate into defect types II and III, carrying a single-negative and single-positive charge, respectively:



Analysis of the IR absorption spectra of MgO single crystals containing residual OH^- however, indicated low concentrations of the OH^- pair defect I [11]. Instead an IR band was observed, characteristic of the H–H stretching mode ν_{HH} of molecular H_2 in solid matrices [13]. The assignment of this band to molecular H_2 on interstitial sites has been confirmed by the ν_{HD} band in MgO single crystals grown from a melt saturated with a D_2O – H_2O mixture [11].

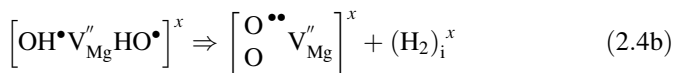
² Square brackets outline the essential parts of the point defects. V stands for vacancy. Subscript i means interstitial and subscripts identify the crystallographic site (except for oxygen sites, where subscripts are omitted). Superscripts prime, dot, and x designate single-negative, positive, and neutral charges, respectively, while double prime and double dot designate double-negative and positive charges, respectively, relative to the unperturbed crystal structure.

The disappearance of most of the OH^- pair defects I from the IR spectrum and appearance of molecular H_2 in the MgO matrix can only be accounted for by assuming a redox conversion:

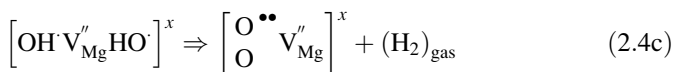


Equation (2.4a) indicates that OH^- pairs at Mg^{2+} vacancy sites change into a peroxy anion, O_2^{2-} , plus molecular H_2 . Peroxy defects can also be described as two adjacent O^{2-} having trapped two holes, converting them into O^- , which then tie a peroxy bond, O^--O^- .

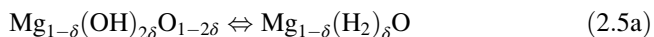
As H_2 molecules are diffusively mobile, even in structurally dense MgO, they can move away, leaving the Mg^{2+} vacancy behind, chargewise compensated by the peroxy anion, O_2^{2-} :



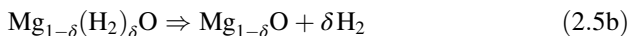
In the case of nanocrystalline MgO, the distance for the interstitial H_2 molecules to diffuse of the nanograins is short, allowing the H_2 to easily degas as demonstrated in Fig. 2.3:



Equation (2.4b) leads to cation-deficient $\text{Mg}_{1-\delta}\text{O}$ with most OH^- converted to H_2 on interstitial sites:



With H_2 diffusing out as of Eq. (2.4c), a non-stoichiometric MgO is left behind:



If $\delta \ll 1$, we may also write the cation-deficient $\text{Mg}_{1-\delta}\text{O}$ as an MgO with excess-oxygen, $\text{MgO}_{1+\delta}$.

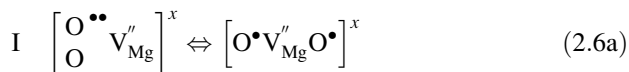
2.3.2 Break-Up of Peroxy Defects and Formation of Positive Holes

Peroxy defects are not unique to MgO. They exist across a range of oxide materials and even seem to be ubiquitous—so much so that it is surprising that their very

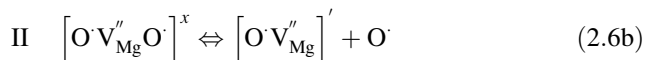
existence has escaped the attention of the scientific community. It is most likely due to their stealth nature, which has made it difficult to detect them and to study their effects on various physical properties of the materials. In order to gain further insight into peroxy defects and how they generate highly mobile positive hole charge carriers, MgO can continue to serve as a model, followed by a discussion of peroxy defects in other matrices, in particular silicates.

The $\text{O}^- - \text{O}^-$ distance in the peroxy defect is only 1.5 Å as compared to 3.0 Å between regular O^{2-} in MgO. With the two O^- spins antiparallel and tightly coupled, the O_2^- entity is diamagnetic. The shortness of the $\text{O}^- - \text{O}^-$ distance suggests a very strong peroxy bond. There are several ways to activate and break it: (1) by heating, (2) by mechanical stress, and (3) by UV light.

Upon heating the $\text{O}^- - \text{O}^-$ bond first loosens up, starting below 200 °C, while staying diamagnetic []. The persistence of diamagnetism suggests that the antiparallel spin coupling is maintained producing a bipolaronic state [5]. Starting around 300 °C paramagnetism begins to develop, following second order kinetics, indicating that the O^- spins start to flip. In combination these two processes comprise Phase I of the two-step peroxy break-up [6]:



The subsequent Phase II, which sets in around 430 °C, leads to the dissociation of the $\text{O}^- - \text{O}^-$ bond and generation of unbound O^- , a mobile positive hole charge carrier, also following a second-order kinetics:



A *condition sine qua non* for the dissociation of the peroxy defect is the transfer of an electron into the already partly broken peroxy bond. The source of this electron is not known, but it can only come from an O^{2-} outside the peroxy defect. The donor O^{2-} thereby turns into O^- , i.e., a positive hole h^\bullet . This positive hole is not spatially close to the Mg^{2+} cation site. Due to slight lattice rearrangements around the $[\text{O} \bullet \text{V}_{\text{Mg}}'']'$ site, which serve to screen its associated negative charge [], this h^\bullet is able to turn into a mobile charge carrier that is free to move away from its “birthplace” and to roam through the solid matrix.

With a band gap as wide as 7.8 eV [14] MgO should be a near-perfect electrical insulator. Indeed, in accordance with the sequence of reactions described by the Eqs. (2.4a, 2.4b, 2.4c)–(2.6a, 2.6b, 2.6c), the electrical conductivity of nominally highest purity MgO single crystals remains low up to about 430 °C, the temperature at which mobile h^\bullet charge carriers appear as a result of the dissociation reaction as given by Eq. (2.6b). The activation energy for the dissociation reaction is ~2.4 eV, while the activation energy for the h^\bullet thus generated is around 1.0 eV [4].

If the dissociation of the peroxy bond requires ~ 2.4 eV, then energies as high as ~ 2.4 eV can be expected to become available when $[\text{O} \cdot \text{V}_{\text{Mg}}'']'$ sites recapture h^\bullet , reconstituting the peroxy defects. Similar amounts of energy may be released through other recombination reactions involving h^\bullet charge carriers.

In the context of luminescence and triboluminescence heating is not of primary interest. More relevant is mechanical action at different levels of stress and different stress rates, including crushing and fracturing. An alternative way to break peroxy bonds is by photodissociation using UV photons of sufficiently high energy. In both cases, mechanical and UV, Step I and Step II coalesce into a single step:

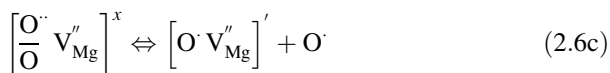


Figure 2.5 (right) depicts the one-step dissociation of a peroxy defect in MgO according to Eq. (2.6c). It leaves the Mg^{2+} vacancy with one O^- and an effective charge of $1-$. The $[\text{O} \cdot \text{V}_{\text{Mg}}'']'$ is depicted as an Mg^{2+} vacancy with the hole state equally spread over its nearest neighbors. This is the V^- center, a paramagnetic site that has been studied extensively by electron spin resonance, ESR, in alkaline earth oxides [15] as well as in many minerals [16].

The positive hole identified as the unbound O^- state, h^\bullet , is shown to the right as a delocalized charge spread over many O^{2-} as indicated by different hues of pink. Evidence for extensive delocalization of the positive hole wavefunction was first derived from the anomaly in the thermal expansion behavior of high purity MgO single crystals and by measurements of the dielectric polarization in an electric field gradient at the limit of 0 Hz [6].

2.3.3 Peroxy Defects in Silica and Silicates

In silica and silicates, peroxy defects are introduced by the same basic redox conversion as in MgO, starting from hydroxyl pairs, $\text{O}_3\text{Si}-\text{OH} \text{ HO}-\text{SiO}_3$, which form peroxy links $\text{O}_3\text{Si}-\text{OO}-\text{SiO}_3$ plus molecular H_2 as illustrated in Fig. 2.6.

While discussing the formation and activation of peroxy defects in MgO, heating was the method of choice to investigate some of the basic properties of peroxy defects. In the context of triboluminescence, the application of stress is more relevant. Stresses can activate peroxy defects by changing the $\text{O}_3\text{Si}-\text{OO}-\text{SiO}_3$ bond angle as illustrated in Fig. 2.7.

To illustrate this further we look at the energy levels of the peroxy entity from a simplified molecular orbital (MO) perspective as illustrated in Fig. 2.8, where we plot the energy as a function of the angle of deformation of the peroxy bond, α . Each O^- has one electron less than the closed-shell configuration of O^{2-} . Hence, a characteristic feature of the $\text{O}^- - \text{O}^-$ bond is that, in the peroxy bond, the strongly antibonding σ -type orbital is empty, which controls the interaction of two adjacent

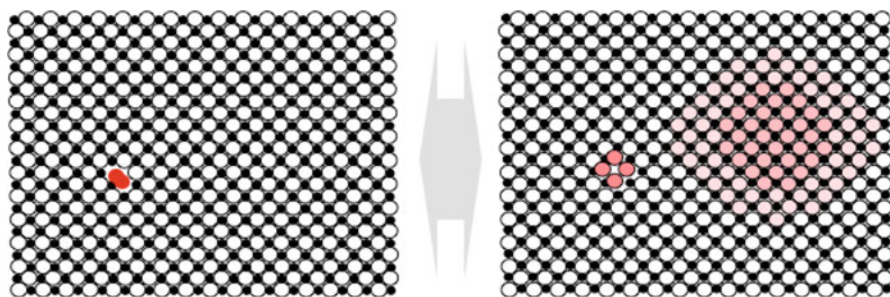


Fig. 2.5 Representation of a peroxy anion (*left*) and a V^- center plus a positive hole (*right*) in the (1 1 0) plane of MgO

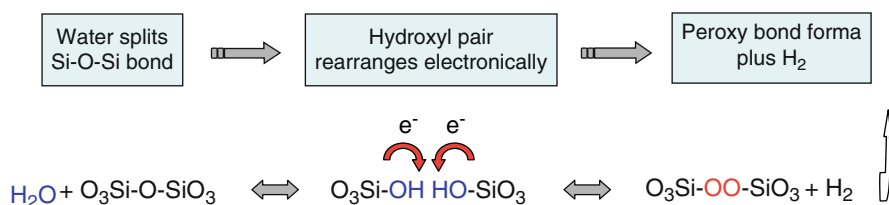


Fig. 2.6 Hydrolysis of an $O_3Si-O-SiO_3$ bond to form an O_3Si-OH pair, which undergoes a redox conversion to a peroxy link, $O_3Si-OO-SiO_3$ plus H_2 . Each step is reversible unless the H_2 diffuses away from the site where it was generated

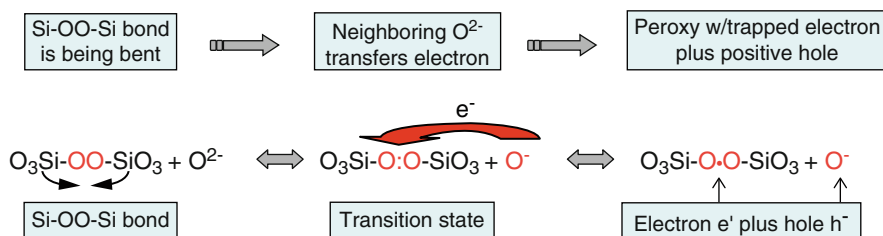


Fig. 2.7 Changing the $O_3Si-OO-SiO_3$ bond causes it to break and for an electron transfer to take place from a nearby O^{2-} . The donor O^{2-} turns into O^- , which becomes a mobile positive hole, while the transferred electron becomes trapped in the broken peroxy bond

O^{2-} and causes them to repel each other. This empty orbital is indicated by a dotted line in Fig. 2.8. Therefore the highest occupied level is now the non-bonding π -type MO formed by the overlap of the O $2p_x$ and $2p_y$ atomic orbitals, if z defined as the direction between the two O^- . This π -type MO is fully occupied with 4 electrons, all of the same energy, as indicated by the solid line at $\alpha = 0$ of the left of Fig. 2.8.

Changing the angle α shifts the energy levels of all MO's. Assuming that the plane of the drawing in Fig. 2.9 is the $x-z$ plane, the MO which derives from O $2p_x$ will destabilize, i.e., its energy will be raised, while the MO which derives from O $2p_y$ will stabilize, i.e., its energy will decrease. At some critical angle α , the

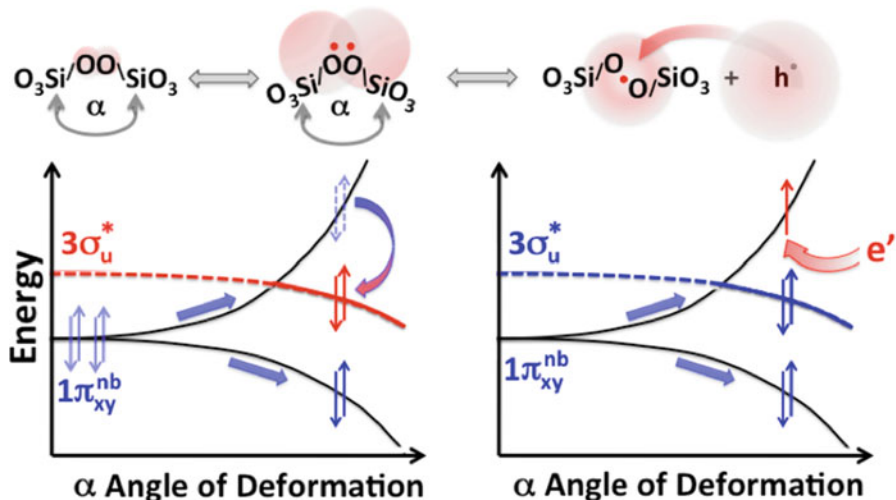


Fig. 2.8 Simplified energy diagram for the highest occupied and the lowest unoccupied molecular orbitals describing the $O_3Si-OO-SiO_3$ bond. As the Si-OO-Si bond angle changes, the relative positions of the energy levels change. Eventually the occupied nonbonding π -type MO crosses the empty antibonding σ -type MO, causing the break-up of the peroxy bond

occupied π -type MO will cross the empty σ -type MO and the electrons will flow from the non-bonding π -type MO into the antibonding σ -type MO, causing the size of the two O^- to suddenly increase. This is the stage equivalent to partly broken peroxy bond as described above by Eq. (2.6a) for O_2^{2-} in MgO.

The right side of Fig. 2.8 retains for illustration purposes the same MO diagram, with the same relative positions of the energy levels, even though there will certainly be substantial changes due to near-instant structural rearrangements and changes in the local geometry around the broken peroxy bond. The right side indicates that an transfer of an electron is taking place from an O^{2-} outside the peroxy defect as described by Eq. (2.6c) for O_2^{2-} in MgO and by Fig. 2.7 for the break-up of the $O_3Si-OO-SiO_3$ bond.

2.3.4 Propagation of the Positive Hole Charge Carriers

As defect electrons in the O^{2-} sublattice, positive holes reside in the O 2sp-type energy levels that form the upper edge of the valence band. Though MgO is among the most ionic oxide materials with the ionicity of the $Mg^{2+}-O^{2-}$ interaction in the 90 % range [17], the residual covalency provides an energetic continuum along which hole states can propagate, roaming through the oxide matrix and even cross grain boundaries.

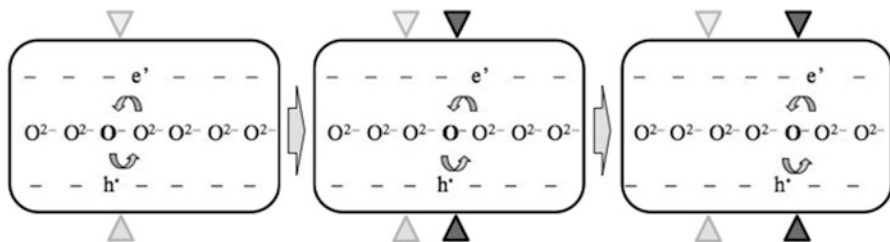


Fig. 2.9 Proposed phonon-assisted electron hopping mechanism for the propagation of positive holes through the bulk of an oxide or silicate material

The structural rearrangements around the broken peroxy bond will affect the reversibility of the reaction and therefore the lifetime of the positive holes states, once they are generated and free to roam through the matrix of the material. The mode of propagation of the positive holes is probably via a phonon-assisted electron hopping mechanism as has been suggested for the delocalization of the hole state over the nearest neighbors of the V^- center in MgO [18].

Figure 2.9 illustrates the phonon-assisted electron hopping mechanism. Assuming that the positive hole can be represented by a point charge, its propagation, say from left to right as indicated in Fig. 2.9, occurs by electrons hopping from right to left. Taking the phonon frequency at ambient temperature to be 10^{12} Hz and the transfer distance at each jump to be 2.8 \AA ($2.8 \times 10^{-10} \text{ m}$), the maximum speed would be $\sim 280 \text{ m/s}$. If the propagation is by random walk, the speed in any one direction will be about 1/3 of this value, $\sim 100 \text{ m/s}$. The measured speed of propagation of stress-activated positive hole charge carriers in laboratory rock samples indicate values in the range [19].

Next the question arises: Where are the peroxy defects located in any given sample so that they can be activated by different levels of stress?

When hydroxyls are introduced into materials, for instance at high temperatures during crystallization from a melt or recrystallization during thermal treatments such as sintering, hydroxyls become invariably incorporated in the host matrix but they are “impurities.” Hence, as thermodynamics requires, during cooling, there will always be a driving force to segregate those impurities and to remove them from the matrix. In polycrystalline materials the most favored sites for segregation are grain boundaries, subgrain boundaries, and dislocations. They all provide local stress release accommodating impurities for which the structure does not provide sites. Hence, impurities such as hydroxyls must segregate.

Figure 2.10 illustrates for a polycrystalline material that, when hydroxyls accumulate on the grain boundaries, many of them will occur in the form of pairs on adjacent grains, directly facing each other. Those hydroxyl pairs will undergo the same type of redox conversion depicted in Fig. 2.6, forming peroxy bonds that straddle the grain boundary. Obviously, such peroxy defects will be extremely sensitive to ever to slight mechanical stresses that tend to shift grains relative to each other. Even sub- \AA shifts are expected to cause an instant break-up of peroxy

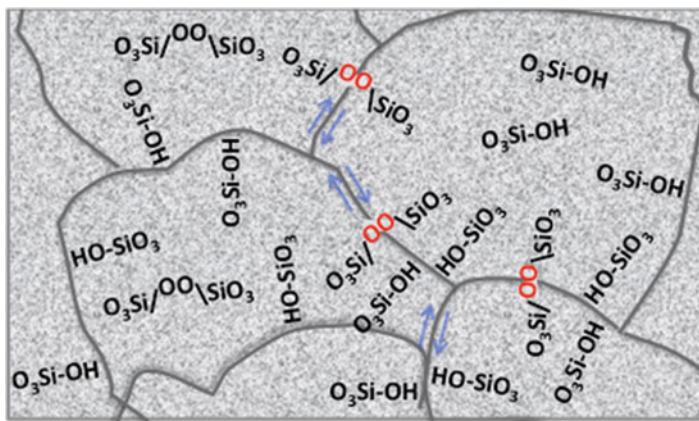


Fig. 2.10 Schematic representation of a polycrystalline silicate material with hydroxyls segregated to the grain boundaries, where many of them occur as hydroxyl pairs. Those hydroxyl pairs will undergo the redox conversion to form peroxy defects, which straddle the grain boundaries and are prone to activation by the slightest shifts between grains

defects and the release of positive hole charge carriers. Something similar would be expected for hydroxyls having segregated to subgrain boundaries and dislocations in single-crystal materials though the required stress levels will be higher.

As mentioned above, due to local structural rearrangements in the neighborhood of broken peroxy bonds, the positive holes are expected to not be able to recombine as readily as they had broken apart. As a result, once activated, positive holes will have wide range of lifetimes allowing them to roam through the bulk of the material.

This can be demonstrated by setting up an experiment as sketched in the inset in Fig. 2.11, taking a finely grained rock tile, here a gabbro, 30 cm × 30 cm × 0.9 cm, fitting it with Cu electrodes around the periphery and in the center, and applying stress at the center via a pair of 5 cm diameter steel pistons [19]. As soon as a load is applied, a positive hole current starts to flow from the center to the periphery. At low loads an initial burst of current is observed, arising from the activation of peroxy defects along grain boundaries, which release their positive holes. While these charge carriers flow out of the stressed rock volume, they also recombine. Thus the magnitude of the initial outflow current is controlled by the balance between the activation and recombination of the positive holes. The faster the stress is applied, the less time is available for the positive holes to recombine. Hence, the outflow current is highest at the fastest stress rates. Figure 2.11 plots the actual currents measured at different stress rates, changing the stress rates over 5 orders of magnitude, while Fig. 2.12 plots the peak current.

Because of differences in the local microscopic environments the lifetimes of the positive holes differ depending on the way stresses are applied. If the stress level is raised suddenly and then kept constant, average lifetimes up to 2 months have been observed. When the stresses are removed, the outflow currents return to zero

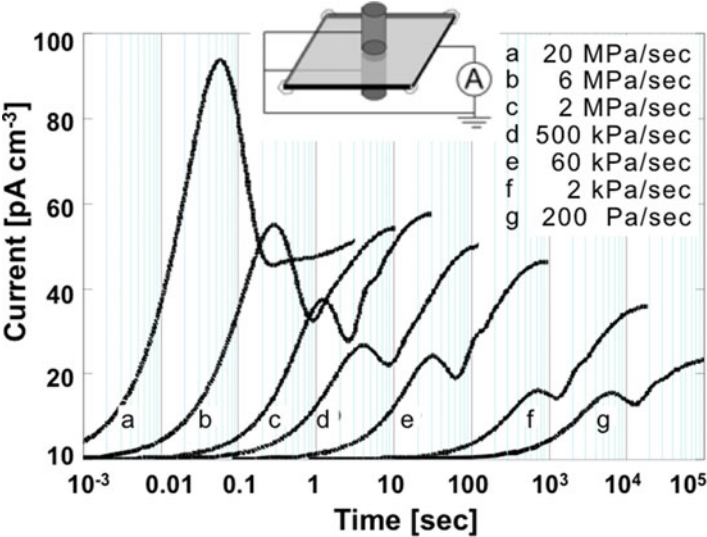
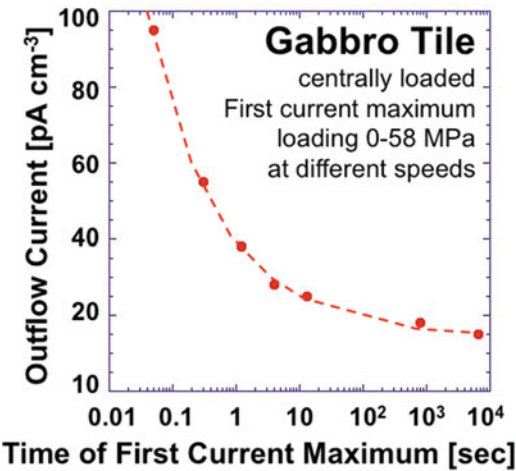


Fig. 2.11 Initial burst of current flowing out of the stressed rock volume, due to the activation of peroxy defects sitting on or straddling grain boundaries and, hence, most sensitive to small stress changes. *Inset:* Sketch of experimental setup

Fig. 2.12 Peak intensity of the initial outflow current at different stress rates, increasing the stress rates over 5 orders of magnitude, indicating a wide spread of lifetimes

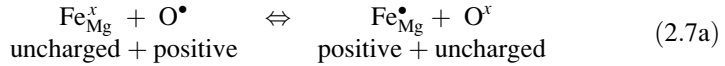


relatively rapidly, though some mobile charge carriers remain active for at least several hours [19].

No information is currently available about triboluminescence during stressing of gabbro, but triboluminescence has been observed during stressing of granite up to near-failure. In this case bursts of light have been reported, increasing in intensity with increasing stress rates and followed by a long afterglow [20].

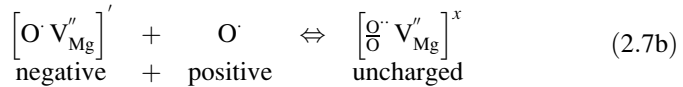
2.3.5 Trapping and Detrapping of Positive Hole Charge Carriers

As positive holes can leave the site, where they have been created and roam through the solid matrix, they can interact with various lattice constituents. If transition metal cations are present in reduced oxidation states such as Fe^{2+} on Mg^{2+} sites in MgO, they can trap the positive holes and turn into Fe^{3+} , if this oxidation reaction is energetically favorable:



where Fe^x and Fe^\bullet stand, respectively, for ferrous (Fe^{2+}) and ferric (Fe^{3+}) on Mg^{2+} sites.

This reaction can be experimentally demonstrated by heating MgO doped with Fe^{2+} and 3d transition metal cations using electron spin resonance (ESR) spectroscopy to measure the amount of Fe^{3+} produced by the reaction given by Eq. (2.7a) proceeding from left to right. In order to oxidize Fe^{2+} to Fe^{3+} MgO containing Fe^{2+} , Mn^{2+} and Cr^{3+} was heated in a stepwise fashion. Above 430 °C, when peroxy defects become unstable and dissociate according to Eqs. (2.6b) and (2.6c), positive holes are released. Those positive holes are then trapped by Fe^{2+} on Mg^{2+} sites, oxidizing them to Fe^{3+} according to Eq. (2.7a) as illustrated by the solid line in Fig. 2.13. In order to maintain the Fe^{3+} in the oxidized state and to be able to record it by ESR spectroscopy, the MgO samples had to be quenched fast to liquid nitrogen temperature, 77 K. Otherwise, upon slow cooling or stepwise cooling, the oxidation reaction reverses as illustrated by the dotted line in Fig. 2.13 with Fe^{3+} self-reducing back to Fe^{2+} [21]. This reaction requires the reconstitution of peroxy bonds according to Eq. (2.7b), which may contribute as much as 2.4 eV to the total energy balance:



Nominally pure MgO single crystals exhibit a bright orange luminescence around 600 nm (2.0 eV), when excited with UV light or high-intensity lasers in the visible region. It has been proposed [22] that this luminescence arises from hole trapping by V^- centers as shown by Eq. (2.7b). Though Duley et al. do not mention the formation of a peroxy entity at the Mg^{2+} vacancy site, the quoted reaction describes the reconstitution of peroxy bonds that had been broken by incident UV photons of sufficiently high energy to cause a direct electron transition from the valence band into the conduction band or by non-linear effects during the absorption of VIS photons during high intensity illumination in the VIS region similar to the Raman effect [23].

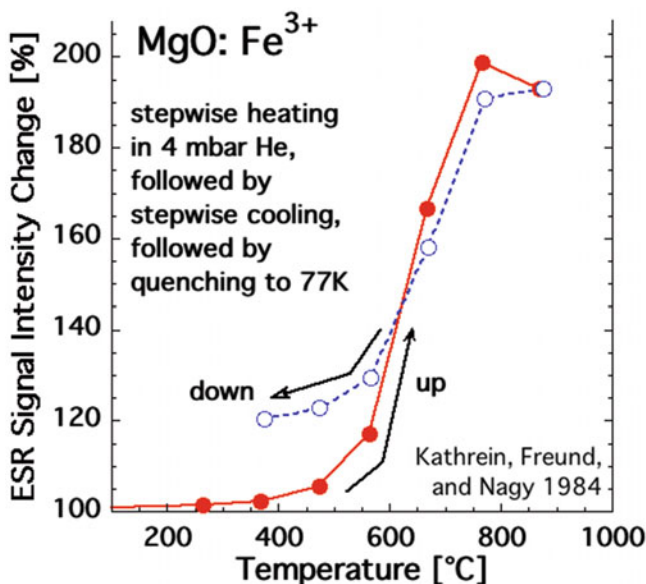


Fig. 2.13 Increase in Fe^{3+} concentration due to trapping of positive holes by Fe^{2+} on Mg^{2+} lattice sites during stepwise heating beyond 430 °C, followed by quenching to 77 K, as indicated by the solid line. During slow or stepwise cooling Fe^{3+} self-reduces to Fe^{2+} as indicated by the dotted line due to peroxy defects able to form again below 430 °C [21]

Similarly, during frictional excitation, triboluminescence of MgO starts at 600 nm (2.0 eV) and peaks around 730 nm (1.7 eV) [24]. Triboluminescence has also been reported to occur during the low temperature and ambient temperature deformation of MgO, CaO, and SrO crystals. Though the nature of the emitting center has not been determined, excitonic transitions from cation vacancy sites are suspected to be involved [25], also pointing at the reconstitution of peroxy defects according to Eq. (2.7b).

Nanosized MgO thin films can be made ferromagnetic by doping them with oxygen, resulting in stoichiometries between MgO and MgO_2 [26]. These films exhibit a strong luminescence at approximately 460 nm (2.7 eV) believed to be due to holes trapped at Mg^{2+} vacancy sites [27]—a suggestion that again points to the reconstitution of peroxy bond according to Eq. (2.7b).

Changing from MgO to CaO, also in the face-centered cubic NaCl-type structure, allows for larger transition metal cations to be incorporated on Ca^{2+} sites. $\text{CaO}:\text{Sn}^{2+}$ exhibits photoluminescence at 490 nm (~2.5 eV) with a very long afterglow when excited at room temperature [28], possibly due to positive holes being trapped and detrapped by Sn^{2+} and the reconstitution of peroxy bonds. Mechanical deformation of nominally pure CaO single crystals introduces an absorption band at 270 nm (4.6 eV), which thermally anneals above 330 °C, and a luminescence band around 450 nm (2.75 eV), which anneals already around room temperature [29]. Any CaO crystals grown from the melt by the carbon fusion

technique will contain peroxy defects analogous to MgO crystals grown by the same technique [11]. Hence, the capability of mechanically deformed CaO and MgO [30] to support luminescence is most likely related to the activation of positive holes and their deactivation through reconstitution of peroxy bonds.

2.4 Luminescence and Triboluminescence in Sulfides and Other Materials

Another way to allow for the incorporation of large transition metal cations is to move from oxide to sulfide materials where the S^{2-} anions have significantly larger ionic radii than O^{2-} . MgS, for instance, crystallizing in the same face-centered cubic NaCl-type structure as MgO, can incorporate rare earth metal cations, providing a rich field of study for optically and thermally stimulated luminescence [31]. The same is true for ZnS-based systems [32–34]. In sulfides the role of the peroxy entity is taken over by disulfide anions, S_2^{2-} , though this analogy is hardly ever mentioned.

However, because the energy levels at the top of the molecular orbital scheme of the S_2^{2-} disulfide and the O_2^{2-} peroxy entities are quite similar, it is to be expected that, in solid sulfides, disulfide entities will be present and also dissociate, releasing hole states into the S^{2-} sublattice, chemically equivalent to S^- . In this case the S^- states will act as charge carriers similar to the O^- states, able to deliver oxidizing potential to distant sites in the sulfide matrix, where transition metal cations such as rare earths reside in low-oxidation states, able to capture the hole and emit photons as part of a luminescent excitation/de-excitation process.

When it comes to organic luminescent materials [35–38], the concept of hole states as mobile charge carriers may also be applied. After all, there are only two basic requirements: (1) that sites should exist, which—upon activation—generate electron-hole pairs, and (2) that the electrons should become trapped and rendered immobile, while the holes would be able to move along the upper edge of the valence band.

2.5 Summary

Triboluminescence is caused by mechanical actions. They may include crushing and fracturing. In this case, highly energetic processes take place on very short time scales during propagation of cracks, leading to the emission of bursts of light from the fracture surfaces and from the space between them. This emission covers a broad spectral range, extending into the UV and possibly into the X-ray region.

If the mechanical actions are more gentle such as during rubbing and tumbling, but nonetheless cause luminescence emerging from within the bulk, the question

arises as to how does such weak mechanical action can lead to luminescence and how does the necessary electronic excitation flow from the surface into the bulk.

The answer may lie in the presence of certain defects in the matrix of oxide materials, which have not been paid the attention they probably deserve: peroxy defects, which consist of pairs of oxygen anions that have changed their valence from 2− to 1−. Under normal conditions the two O[−] are tightly coupled and strictly localized, forming a very short O[−]–O[−] bond. However, this peroxy bond is also very labile. Slight variations in the local environment can cause the peroxy bonds to break, even transient perturbations by sound waves. When this happens, electron-hole pairs are generated with the electrons trapped in the broken peroxy bonds and the holes turning into highly mobile charge carriers, “positive holes.” Those positive holes have the ability to flow away from the sites where they had been generated, propagating via a phonon-assisted electron hopping mechanism at speeds up to about 100 m/s, traveling far afield.

Chemically, the positive holes represent O[−] in a matrix of O^{2−}. They have a strong propensity to take over one additional electron. This means that they are strongly oxidizing, able to oxidize transition metal cations, which they may encounter as they roam through the matrix of the oxide materials. Such oxidation reactions are often strongly exothermal, causing the transition metal cations to become electronically excited. If they radiatively de-excite, luminescence will occur.

Positive holes can also recombine with broken peroxy bonds, reconstituting the peroxy defects. It is known that the activation energy required to dissociate peroxy bonds in MgO is ~2.4 eV [4] and probably of similar values in other oxide matrices. Hence, the recombination of a positive hole with a broken peroxy bond may yield energies up to ~2.4 eV. If the recombination takes place at a site of a transition metal cation, this energy might be transferred from the newly forming peroxy defect onto the transition metal cation, causing it to become electronically excited, able to subsequently de-excite by emitting a luminescence photon.

Acknowledgments The early part of this work was supported by the Deutsche Forschungsgemeinschaft in Germany, and the latter part primarily by NSF and NASA. Current support by NASA is provided by the grant #NNX12AL71G. I thank many students and coworkers who participated in this research and helped me develop the knowledge base, on which this chapter is based. Their names are listed as coauthors in the references given below.

References

1. Langford, S. C., & Dickinson, J. T. (2009). Emission of particles and photons from the fracture of minerals and inorganic materials. In *Spectroscopic characterization of minerals and their surfaces* (pp 224–244). ACS Symposium Series, Vol. 415, Chapter 12, doi: 10.1021/bk-1990-0415.ch012.
2. Kittel, C. (1996). *Introduction to solid state physics* (7th ed.). New York: Wiley.
3. Griscom, D. L. (1990). Electron spin resonance. *Glass Science and Technology*, 48, 151–251.

4. Kathrein, H., & Freund, F. (1983). Electrical conductivity of magnesium oxide single crystal below 1200 K. *Journal of Physics and Chemistry of Solids*, 44, 177–186.
5. Batllo, F., LeRoy, R. C., Parvin, K., Freund, F., & Freund, M. M. (1991). Positive hole centers in magnesium oxide—correlation between magnetic susceptibility, dielectric anomalies and electric conductivity. *Journal of Applied Physics*, 69, 6031–6033.
6. Freund, F., Freund, M. M., & Batllo, F. (1993). Critical review of electrical conductivity measurements and charge distribution analysis of magnesium oxide. *Journal of Geophysical Research*, 98(B12), 22209–22229.
7. Martens, R., Gentsch, H., & Freund, F. (1976). Hydrogen release during the thermal decomposition of magnesium hydroxide to magnesium oxide. *Journal of Catalysis*, 44, 366–372.
8. Freund, F., Scheikh-ol-Eslami, N., & Gentsch, H. (1975). Formation of O^- centers by homolytic decomposition of OH^- groups on magnesium oxide. *Angewandte Chemie, International Edition*, 14(8), 568–569.
9. Freund, T., Martens, R., & Scheikh-ol-Eslami, N. (1975). Recrystallization effect during the dehydration of magnesium hydroxide. *Journal of Thermal Analysis*, 8(3), 525–529.
10. Freund, F., & Sperling, V. (1976). A magnesium oxide defect structure of hexagonal symmetry. *Materials Research Bulletin*, 11, 621–630.
11. Freund, F., & Wengeler, H. (1982). The infrared spectrum of OH-compensated defect sites in C-doped MgO and CaO single crystals. *Journal of Physics and Chemistry of Solids*, 43, 129–145.
12. Kröger, F. A. (1964). *The chemistry of imperfect crystals*. Amsterdam: North-Holland.
13. Krieger, R. J., & Welsh, H. L. (1968). The induced infrared fundamental band of hydrogen dissolved in solid argon. *Canadian Journal of Physics*, 46(10), 1181–1189. doi:[10.1139/p68-151](https://doi.org/10.1139/p68-151).
14. Taurian, O. E., Springborg, M., & Christensen, N. E. (1985). Self-consistent electronic structures of MgO and SrO. *Solid State Communications*, 55(4), 351–355.
15. Henderson, B., & Wertz, J. E. (1977). *Defects in the alkaline earth oxides*. London: Taylor & Francis.
16. Marfunin, A. S. (1979). *Spectroscopy, luminescence and radiation centers in minerals* (pp. 257–262). New York: Springer Verlag.
17. Pacchioni, G., Sousa, C., Illas, F., Parmigiani, F., & Bagus, P. S. (1993). Measures of ionicity of alkaline-earth oxides from the analysis of ab initio cluster wave functions. *Physical Review B*, 48, 11573–11582.
18. Shluger, A. L., Heifets, E. N., Gale, J. D., & Catlow, C. R. A. (1992). Theoretical simulation of localized holes in MgO. *Journal of Physics: Condensed Matter*, 4(26), 5711–5722.
19. Scoville, J., Sornette, J., & Freund, F. T. (2015). Paradox of peroxy defects and positive holes in rocks: Part II. Outflow of electric currents from stressed rocks. *Journal of Asian Earth Sciences*, 114(Part 2), 338–351.
20. Maeda, I. (1986). Activities of triboluminescence at sample failure of granite. *Journal of the Faculty of Science, Hokkaido University. Series 7, Geophysics*, 8(1), 65–81.
21. Kathrein, H., Freund, F., & Nagy, J. (1984). O^- -ions and their relation to traces of H_2O and CO_2 magnesium oxide: an EPR study. *Journal of Physics and Chemistry of Solids*, 45, 1155–1163.
22. Duley, W. W., & Rosatzin, M. (1985). The orange luminescence band in MgO crystals. *Journal of Physics and Chemistry of Solids*, 46(2), 165–170.
23. Harris, D. C., & Bertolucci, M. D. (1989). *Symmetry and spectroscopy: An introduction to vibrational and electronic spectroscopy*. New York: Dover Publications.
24. Miura, T., Hosobuchi, E., & Arakawa, I. (2009). Spectroscopic studies of triboluminescence from a sliding contact between diamond, SiO_2 , MgO, NaCl, and Al_2O_3 (0001). *Vacuum*, 84(5), 573–577.
25. Williams, G. P., & Turner, T. J. (1979). Triboluminescence in single crystal alkaline earth oxides. *Solid State Communications*, 29, 3.

26. Mahadeva, S. K., Jincheng Fan, A. B., Sreelatha, K. S., Lyubov, B., & Rao, K. V. (2013). Magnetism of amorphous and nano-crystallized Dc-sputter-deposited MgO thin films. *Nanomaterials*, 3, 486–497.
27. Martínez-Boubeta, C., Martíneza, A., Hernández, S., Pellegrino, P., Antony, A., Bertomeu, J., et al. (2011). Blue luminescence at room temperature in defective MgO films. *Solid State Communications*, 151(10), 751–753.
28. Donker, H., Smit, W. M. A., & Blasse, G. (1987). On the luminescence of $\text{CaO}:\text{Sn}^{2+}$. *Physica Status Solidi*, 145(1), 333–342.
29. Gonzalez, R., Chen, C. B. Y., Liu, H., Williams, G. P., Jr., Rosenblatt, G. H., Williams, R. T., et al. (1993). Luminescence properties of deformed CaO crystals. *Physical Review B*, 47, 4910.
30. Melton, R., Daniele, N., & Turner, T. J. (1980). Luminescence of MgO during mechanical deformation. *Physica Status Solidi A*, 57(2), 755–764.
31. Chakrabarti, K., Mathur, V. K., Rhodes, J. F., & Abbundi, R. J. (1988). Stimulated luminescence in rare-earth-doped MgS. *Journal of Applied Physics*, 64, 1363–1366.
32. Aich, N., Appalla, A., Saleh, N. B., & Ziehl, P. (2013). Triboluminescence for distributed damage assessment in cement-based materials. *Journal of Intelligent Material Systems and Structures*, 24(14), 1714–1721.
33. Bergeron, N. P., Hollerman, W. A., Goedeke, S. M., Hovater, M., Hubbs, W., Finchum, A., et al. (2006). Experimental evidence of triboluminescence induced by hypervelocity impact. *International Journal of Impact Engineering*, 33, 91–99.
34. Fontenot, R. S., Hollerman, W. A., Bhat, K. N., & Aggarwal, M. D. (2012). Comparison of the triboluminescent properties for europium tetrakis and $\text{ZnS}:\text{Mn}$ powders. *Journal of Theoretical and Applied Physics*, 6, 15.
35. Blasse, G., & Grabmaier, B. C. (1994). *Luminescent materials*. New York: Springer.
36. Chandra, B. P., & Zink, J. I. (1980). Mechanical characteristics and mechanism of the triboluminescence of fluorescent molecular crystals. *Journal of Chemical Physics*, 73(12), 5933–5941.
37. Wang, J., Zhang, M., Zhang, Q., Ding, W., & Su, Q. (2007). The photoluminescence and thermoluminescence properties of novel green long-lasting phosphorescence materials $\text{Ca}_8\text{Mg}(\text{SiO}_4)_4\text{Cl}_2:\text{Eu}^{2+}, \text{Nd}^{3+}$. *Applied Physics B*, 87(2), 249–254.
38. Teotonio, E. E. S., Fett, G. M., Brito, H. F., Faustino, W. M., de Sa, G. F., Felinto, C. F. C., et al. (2008). Evaluation of intramolecular energy transfer process in the lanthanide(III) bis- and tris-(TTA) complexes: Photoluminescent and triboluminescent behavior. *Journal of Luminescence*, 128, 193–198.

Triboluminescence

Theory, Synthesis, and Application

Olawale, D.O.; Okoli, O.O.I.; Fontenot, R.S.; Hollerman,
W.A. (Eds.)

2016, VIII, 454 p. 335 illus., 235 illus. in color.,

Hardcover

ISBN: 978-3-319-38841-0